THE JOURNAL OF PHYSICAL CHEMISTRY Letters

Letter

Cite This: J. Phys. Chem. Lett. 2017, 8, 5648-5655

pubs.acs.org/JPCL

Singular Value Decomposition Method to Determine Distance Distributions in Pulsed Dipolar Electron Spin Resonance

Madhur Srivastava[†,‡] and Jack H. Freed*[,†,§]

[†]National Biomedical Center for Advanced ESR Technology, [‡]Meinig School of Biomedical Engineering, and [§]Department of Chemistry and Chemical Biology, Cornell University, Ithaca, New York 14853, United States

Supporting Information

ABSTRACT: Regularization is often utilized to elicit the desired physical results from experimental data. The recent development of a denoising procedure yielding about 2 orders of magnitude in improvement in SNR obviates the need for regularization, which achieves a compromise between canceling effects of noise and obtaining an estimate of the desired physical results. We show how singular value decomposition (SVD) can be employed directly on the denoised data, using pulse dipolar electron spin resonance experiments as an example. Such experiments are useful in measuring distances and their distributions, $P(r)$ between spin labels on proteins. In noise-free model cases exact results are obtained, but even a small amount of noise (e.g., SNR = 850 after denoising) corrupts the solution. We develop criteria that precisely determine an optimum approximate solution, which can readily be automated. This method is applicable to any signal that is currently processed with regularization of its SVD analysis.

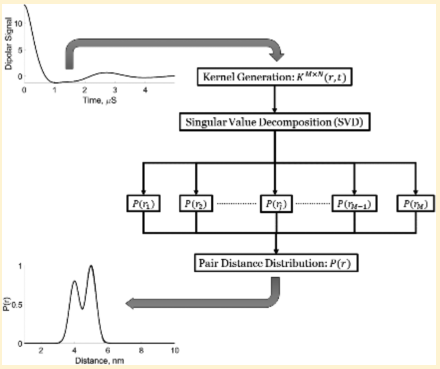

Many physical techniques require that the original experimental signal be processed to yield the desired results.[1−6] In such cases, a regularization method, such as Tikhonov regularization,[7−11] is often employed to strike a balance between canceling undesirable effects of noise in the signal and providing a useful approximation to the desired experimental results. The regularization is usually incorporated with singular-value decomposition (SVD),[7,12] which, however, would be seriously noise-corrupted without regularization.

Here, we describe a new approach which does not depend on the compromise of a regularization method, so it is able to yield significantly more accurate results. We have previously introduced a wavelet-based denoising method which provides SNR improvement of about 2 orders of magnitude.[13,14] Our new SVD approach reported here benefits from such initial denoising. We illustrate the method by applying it to pulse dipolar ESR (PDS) experiments, which have in recent years been shown to be important in determining distance distributions and structures in many proteins.[2,15−23] However, it would be applicable to any signal that currently requires regularization of its SVD analysis.

Our presentation consists of the following aspects: (1) We first show how a careful analysis of the SVD solution yields the exact result for noise-free models. (2) Then we show that even very small amounts of noise (e.g., SNR ≈ 850) are sufficient to corrupt this, but we develop a precise criterion to determine which singular value contributions (SVCs) must be kept and which discarded to obtain a useful solution. (3) However, even such a solution typically contains spurious defects, requiring a further refinement of the method that we call *segmentation*. That is, for example, for PDS, one obtains a time-dependent signal, $S(t)$, from which a distance distribution $P(r)$ is extracted. It turns out, especially in the presence of finite noise, that the SVD convergence properties are dependent on r, so that one must apply our method in an r-dependent fashion. This may be implemented in a practical manner in terms of a few segments of r. (4) We find that this method leads to a highly accurate $P(r)$ without spurious peaks, limited only by the residual noise, and it is more accurate than can be achieved using a regularization approach even on the (mostly) denoised signal (cf. Figures S9−S12).

The distance distribution between an ensemble of spin pairs obtained from the PDS signal may be expressed as a Fredholm Equation of the first kind as

$$\int_{R_{min}}^{R_{max}} \kappa(r, t)P(r)\, dr = S(t) \tag{1}$$

where $\kappa(r, t)$ is the kernel representing the dipolar interaction of a spin-pair at a given r that has been integrated over all possible orientations of r with respect to the large magnetic field defining the lab frame; $P(r)$ is the distance distribution between the spin pairs; and $S(t)$ is the dipolar signal. Equation 1 is discretized in matrix form as follows:

$$KP = S \tag{2}$$

where K is an $M \times N$ matrix, with M the dimension of the discrete values of S and N of P, and $N \leq M$. The PDS experiment measures the dipolar signal $S(t)$. Solving eq 2 for P is an ill-posed problem because the kernel matrix K is singular

Received: September 7, 2017
Accepted: November 3, 2017
Published: November 3, 2017

DOI: 10.1021/acs.jpclett.7b02379
J. Phys. Chem. Lett. 2017, 8, 5648−5655

Scheme 1. Block Diagram Showing the Determination of Distance Distributions from Pulsed Dipolar Spectroscopy Using (A) Tikhonov Regularization and (B) the New Singular Value Decomposition Method

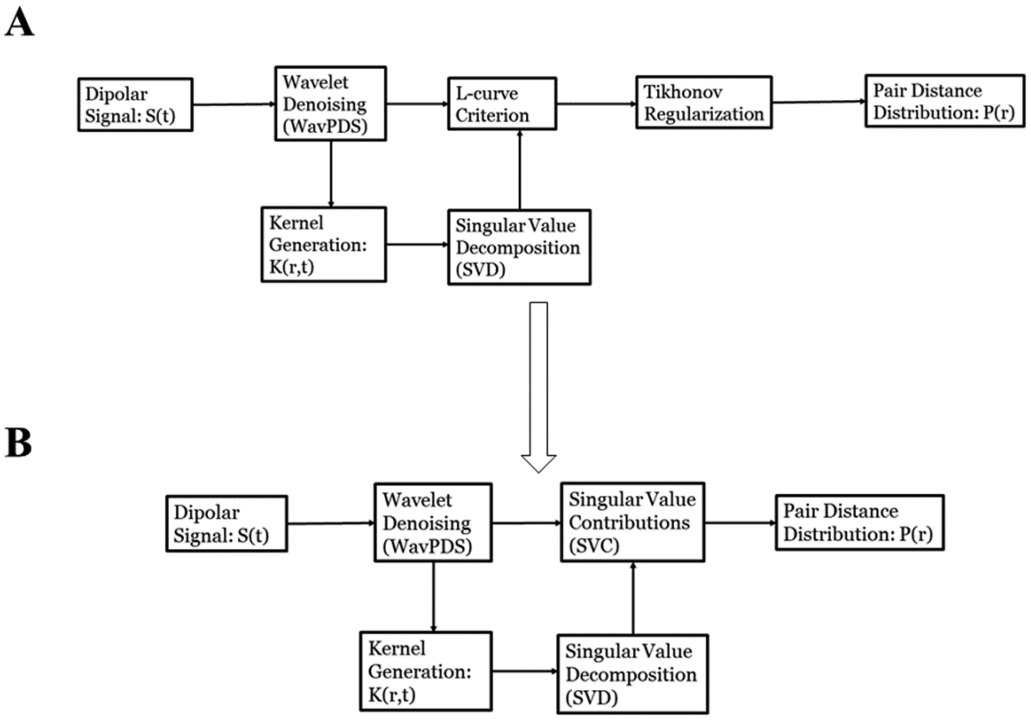

(or nearly so), that is, its rank $k < M$. Furthermore, $S(t)$ contains noise, increasing the challenge of obtaining a reliable $P(r)$.

Thus, as commented above, one usually resorts to regularization or model fitting methods to obtain reasonable results for $P(r)$, and the method of Tikhonov regularization (TIKR) is commonly used.[7,9] However, it relies heavily on the selection of the regularization parameter (λ), which yields a compromise between a reliable fit to the data in a least-squares sense and maintaining stability of the $P(r)$.[7,9,24] For a noisy dipolar signal, the TIKR method compromises on resolution in order to avoid an unstable $P(r)$. Moreover, this procedure is vulnerable to the appearance of spurious peaks and negative values for $P(r)$, due in part to noise in the dipolar signal.

Model fitting methods that are also used[9,23,25−35] require, on the other hand, *a priori* model functions to estimate $P(r)$, which may not accurately represent the actual distance distributions. This becomes especially true if the $P(r)$ is multimodal. Model fitting methods, as well as TIKR, are frequently unable to differentiate between intrinsically nonoverlapping peaks that are significantly broadened by the needs of the methodology, as well as by highly "dynamical" systems characterized by a broad distance distribution when frozen.

We now describe our *objective* method (which can be easily automated) based on SVD to resolve such matters. It yields accurate distance distributions with high resolution and without spurious peaks or negative $P(r)$'s, without resorting to regularization or model fitting. The dipolar signal is first denoised using our recently developed WavPDS method[14] based on wavelet transforms.[36] (Alternatively, a signal already with high SNR, e.g., from signal averaging, could skip this first step). This denoised signal is then directly converted into the $P(r)$ by our new SVD approach. This scheme is shown in Scheme 1 and compared with the method using Tikhonov regularization.

In its basic form, the SVD of the "Kernel" matrix K can be obtained as $K = U\Sigma V^T$ so eq 2 can be rewritten as,[7]

$$U\Sigma V^T P = S \tag{3}$$

where U is an $M \times M$ column-orthogonal matrix, V is an $N \times N$ column-orthogonal matrix, and Σ is an $M \times N$ diagonal matrix containing the non-negative singular values, σ_i (where i = 1, 2, ..., N) in decreasing order.[37]

To obtain P, using the SVD in eq 3, one has

$$P = V\Sigma^{-1}U^T S \tag{4}$$

where Σ^{-1} represents the diagonal matrix containing the reciprocal of the singular values. Then eq 4 can be rewritten in discretized form as

$$P_j = \sum_{i=1}^{k}\sum_{l=1}^{M} V_{ji}(\Sigma^{-1})_{ii}U^T{}_{il}S_l \tag{5}$$

where j is the index representing distance r, l is the index representing time t, and i is the index representing the singular values. The sum is only over the k positive nonzero σ_i's, where k is the rank of K, whereas the $N - k$ remaining σ_i's should be zero representing their linear dependence. Thus, one can, in principle, completely characterize the solution P by an analysis of the singular value contributions (SVCs): $\frac{V_{ji}U^T{}_{il}S_l}{\sigma_i}$ in the sum of eq 5, where $(\Sigma^{-1})_{ii} = \frac{1}{\sigma_i}$, for the nonzero σ_i's. However, in practice, it is difficult to determine k for the ill-posed problem even with a noise-free signal, due to computational round-off noise, so that the $(N - k)$ singular values are not precisely zero. To obtain a good solution P, a metric is needed to determine the cutoff value for the σ_i.

One such approach is simply to start with just the SVC from the largest singular value (SV) in eq 5. Then sequentially add

DOI: 10.1021/acs.jpclett.7b02379
J. Phys. Chem. Lett. 2017, 8, 5648−5655

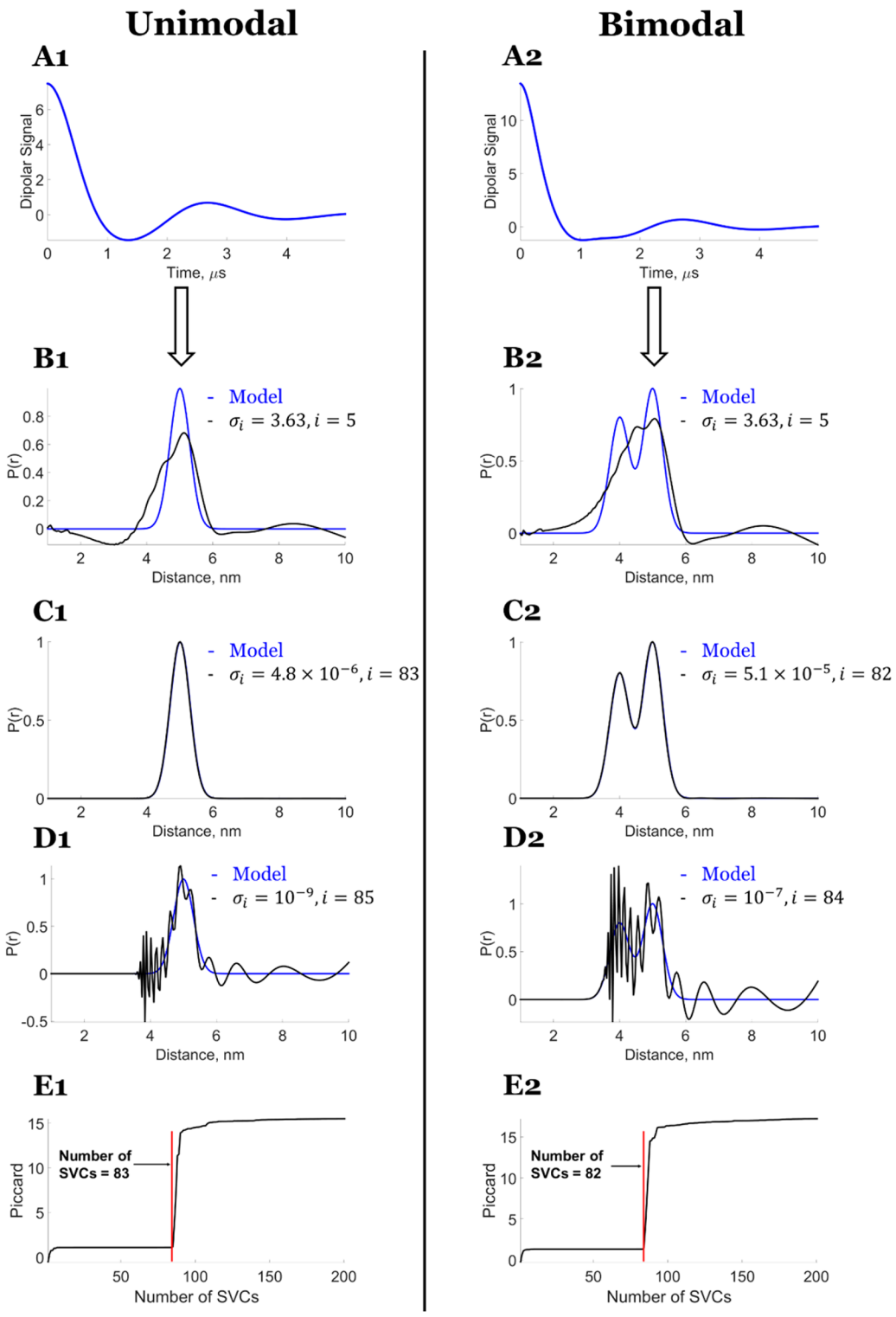

Figure 1. Model Data: The exact solution using the SVD method; $P(r)$ vs number of singular value contributions (SVCs). Unimodal Distance Distribution: (A1) Noise-free dipolar signal. Comparison of model distribution with $P(r)$ generated from (B1) fewer SVCs $i = 3$, $\sigma_i = 8.04$; (C1) exact solution obtained for $i = 83$, $\sigma_i = 4.8 \times 10^{-6}$; (D1) more SVCs $i = 85$, $\sigma_i = 10^{-9}$; (E1) Piccard plot of log_{10} $(\sum_i |u_i^T S/\sigma_i|^2)$ vs the number of singular values from $i = 1$ to 200 starting from largest value; it shows the contributions of singular values that lead to stable and unstable distributions. Bimodal Distance Distribution: (A2) noise-free dipolar signal. Comparison of model distribution with $P(r)$ generated from (B2) fewer SVCs $i = 3$, $\sigma_i = 8.04$; (C2) exact solution obtained for $i = 82$, $\sigma_i = 5.1 \times 10^{-5}$; (D2) more SVCs $i = 84$, $\sigma_i = 10^{-7}$; (E2) Piccard plot of log_{10} $(\sum_i |u_i^T S/\sigma_i|^2)$ vs the number of singular values from $i = 1$ to 200 starting from largest value; it shows the contributions of singular values that lead to stable and unstable distributions.

the SVC's from successively smaller SV's while monitoring the ith approximation to P_j given by eq 5. As one does this the $P(r)$ becomes better approximated. We illustrate this in Figure 1 for the ideal cases of noise-free $P(r)$ models of (1) unimodal and

DOI: 10.1021/acs.jpclett.7b02379
J. Phys. Chem. Lett. 2017, 8, 5648−5655

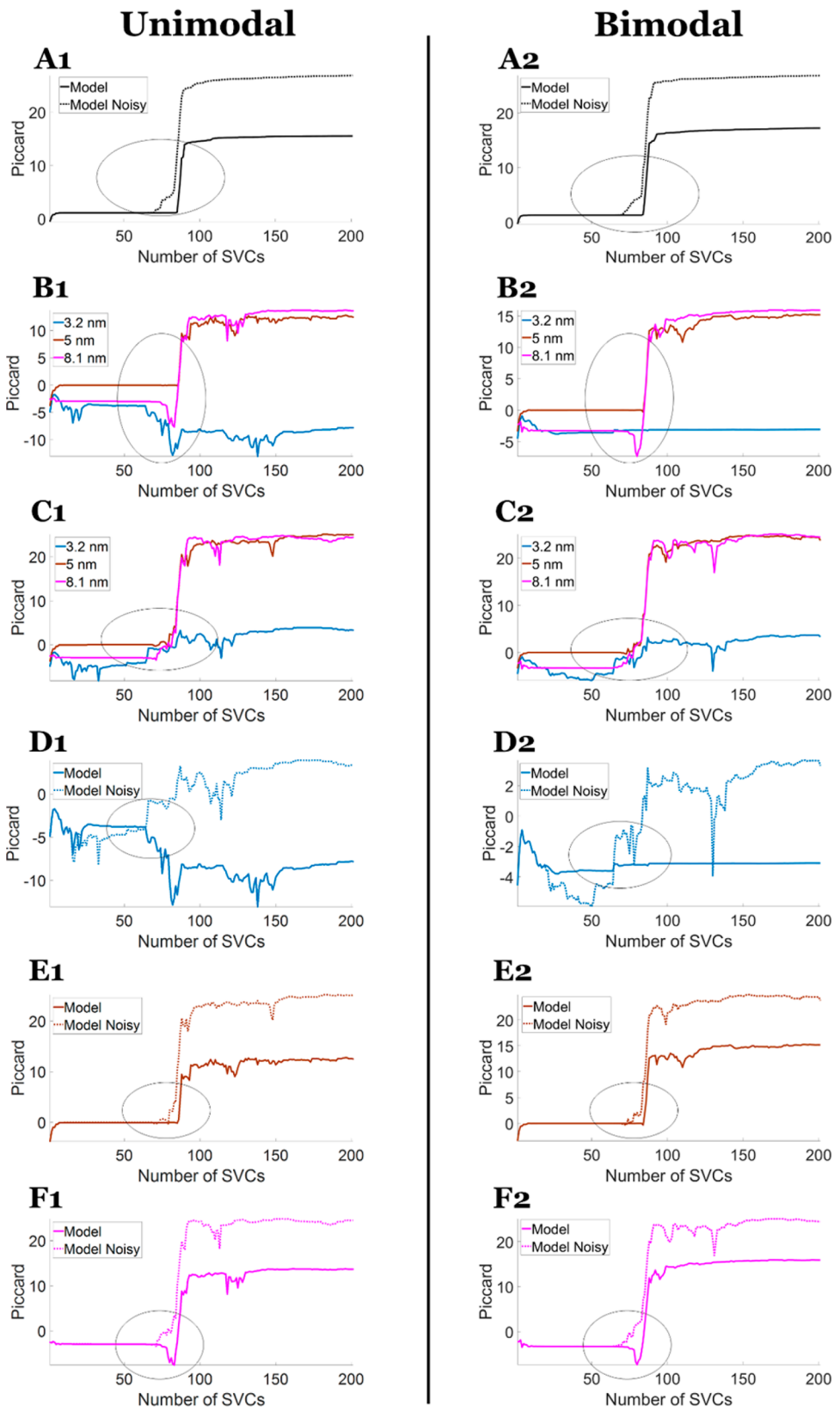

Figure 2. Piccard plots of log_{10} $(\sum_i |u_i^T S/\sigma_i|^2)$ comparing noise-free and some noise (SNR = 850) cases for different distance segments. Case 1 is unimodal and Case 2 is the bimodal model. (A) Piccard plots for noise-free vs some noise. (B) Comparison of distance (r) dependent Piccard plots at 3.2 nm, 5 nm, and 8.1 nm for noise-free models. (C) Same as B, except for models with some noise. Comparison of distance (r) dependent Piccard plots for noise-free vs some noise cases for (D) 3.2 nm, (E) 5 nm, and (F) 8.1 nm.

(2) bimodal distributions. Here A1 and A2 show their dipolar signals in the time domain. The B1 and B2 compare the approximations to $P(r)$ after just 5 SVC's to the model shown in blue. The C1 and C2 show the $P(r)$ when they have

DOI: 10.1021/acs.jpclett.7b02379
J. Phys. Chem. Lett. 2017, 8, 5648−5655

converged to the exact result for i = 83 and 82, respectively, whereas D1 and D2 show the divergent results for $P(r)$ with just two additional SVC's. Thus, one method is to add SVC's sequentially and to the stop just before additional SVC's lead to diverging results. This is shown in more detail in the SI Figures S4 and S6. In fact, these results are fully consistent with the theorem[12] stating the necessary and sufficient conditions for obtaining the exact results by SVD, that is given in the SI and illustrated in Figures S1 and S2.

There is a second approach to determining the cutoff value for the SVC's. This is based on the Piccard condition,[7,38] which requires that in order for eq 5 to have a solution, it is necessary and sufficient that

$$[\text{Piccard}] \equiv \sum_{i=1}^{q} \frac{1}{\sigma_i^2} |\langle S, u_i \rangle|^2 < \infty, \quad \text{where } q \leq k < M \tag{6}$$

where $\langle S, u_i \rangle$ is the inner product of the two vectors, and u_i is the ith column of the column-orthogonal matrix U. The Piccard condition states that to obtain a desirable solution, eq 6 should converge to a finite value, which is represented by less than ∞ sign. It also informs one when a particular solution begins to diverge with the addition of further singular values. For the noise-free examples, we are first addressing, we can expect $q = k$ is satisfactory but $q > k$ is not. This is shown in Figure 1, E1 and E2, which show that the (log of the) Piccard sum diverges at the number of SVC's exactly where the $P(r)$ approximations become distorted. Thus, one can use the cutoff value of i as that just before the Piccard plot diverges.

If only a small amount of noise is added (we use a nominal value of SNR = 850, which is consistent with our denoising capabilities[14]), then the necessary and sufficient conditions of the theorem are no longer satisfied, as also illustrated in Figures S1 and S2; so the SVD can only be used to obtain a best fit in a least-squares sense.[12] Also, in the presence of even such modest noise not only must one cut off the sum of SVC's in eq 5 sooner, but additionally there is no longer a precise cutoff for the SVC's as shown in the Piccard plots of Figures 2 A1 and A2; there is a blurring of this cutoff as is illustrated further in plots of $P(r)$ vs added SVC's shown in Figures S5 and S7 for SNR = 850.

We have found that this is due to the fact that a good choice of cutoff becomes dependent upon the value of r, and this is illustrated in Figure 2 for Piccard plots done separately for r = 3.2, 5, and 8.1 nm. For a noise-free signal, in Figure 2, B1 and B2, one can see that different values of r diverge at about the same singular value cutoff or have already converged and remain so, (e.g., r = 3.2). However, there is a change once noise is present. Then each r value diverges at different singular value cut-offs (cf. Figure 2 C1 and C2) in addition to the fact that the cut-offs occur sooner as a function of i than in the noise-free case (cf. Figure 2, E1, E2, F1, and F2). In Figure 2, D1 and D2 at 3.2 nm, the Piccard plot for a noisy dipolar signal diverges at σ_i = 0.2, whereas for the noise-free signal it remains converged. It can also be seen from Figure 2, that shorter distances diverge sooner than longer distances. Scheme 2 shows the block diagram of the SVD based approach using different SVCs for different r_j values, such that $q \rightarrow q_j$. If this fact is ignored, spurious peaks and other defects will arise as illustrated in the SI (Figures S9–S12 and below).

Scheme 2. Block Diagram Showing Generation of Probability Values at Each Distance Measurement[a]

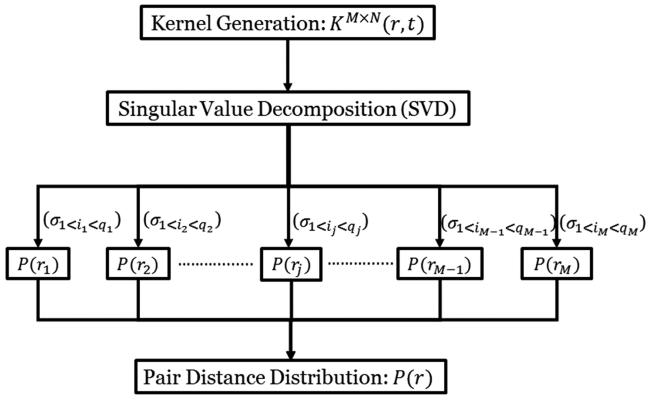

[a]For practical analyses, it is sufficient to consider just 3 or 4 ranges (cf. Figures 3 and S8.

Therefore, in principle, one needs to construct the P_j for each r_j value separately using eq 5. Equation 5 can thus be rewritten to represent this approach as

$$P_j = \sum_{l=1}^{M} \sum_{i=1}^{q(j)} V_{ji} (\Sigma^{-1})_{ii} U^T{}_{il} S_l \tag{7}$$

However, more practically one can use just 3 or 4 segments of r as illustrated in Figures 3D and S8. Within each of these segments, the Piccard expression diverges just after the correct q_j is reached as shown in Figures S13–S20. In a few cases, some r values in a segment do not yet diverge at this cutoff (Figures S14 and S18), but they have reached their converged value such that the contribution of the subsequent $(q + 1)$th singular value is negligible. The singular value cutoff is usually taken at the first r value of the segment that diverges. Remaining r values, although not yet diverged, have typically achieved their convergence (see flat lines in Figures S14 and S18). It is this property that enables the segmentation approach. Of course, one can further divide that segment into two or more segments and select their respective singular value cut-offs, but we find it is unnecessary. In some cases, especially at short distances for which $P(r) = 0$ (e.g., Figures S13 and S17), divergence occurs after only a very few SVCs. We have noticed that the presence of noise in the dipolar signal severely affects the short distances where $P(r) = 0$. One can see in the insets to Figures S13 and S17 that the Piccard plot in the segment diverges from just the first SVC to the second SVC. In Figure S13, the Piccard plots further diverge at later SVC. This subsequent divergence clearly is not important.

To obtain appropriate segmentation and singular value cutoff for each segment, one first performs the sum of eq 5 starting from the largest singular value with the whole distribution taken as a single segment. SVCs are sequentially added in the order of decreasing singular values until the ith SVC yields an unstable approximation to $P(r)$ for a given region of r. That region of r becomes the first segment with no further SVCs needed. SVCs are then added for the remaining r region(s) until another region of r become unstable. This process is repeated until convergence for all the regions of r is achieved. This SVC approach leads to a good approximation of $P(r)$ without spurious peaks.

DOI: 10.1021/acs.jpclett.7b02379
J. Phys. Chem. Lett. 2017, 8, 5648–5655

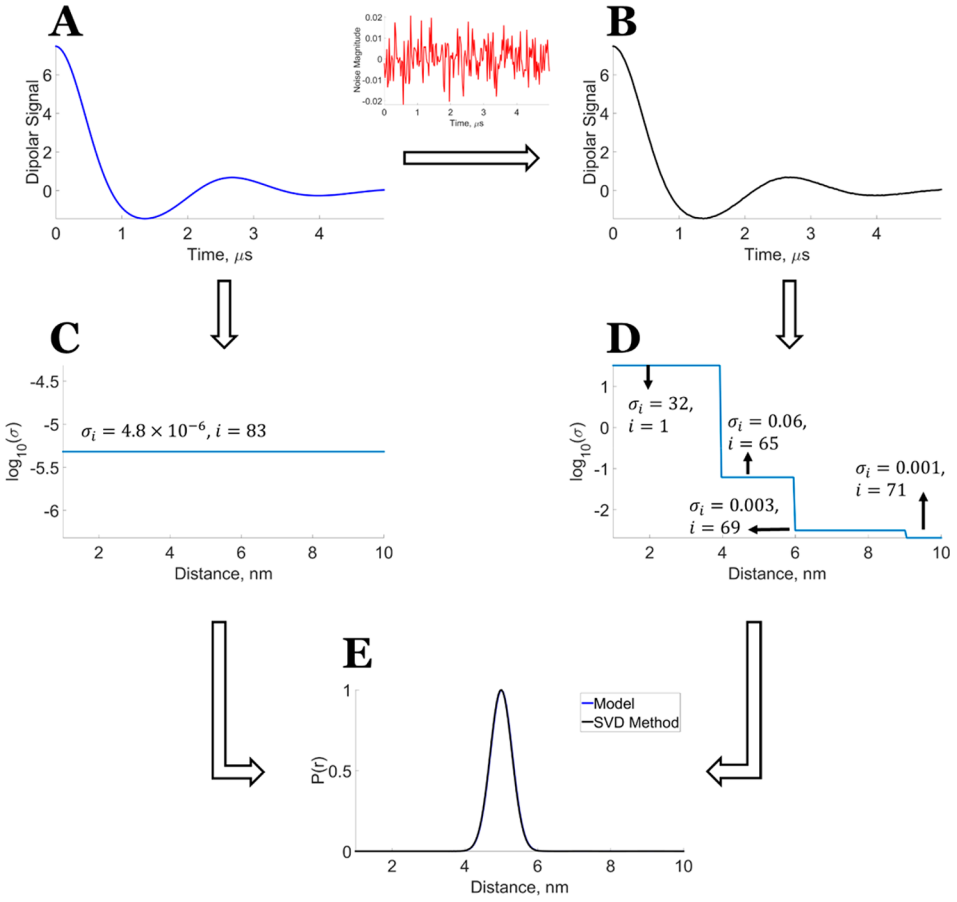

Figure 3. Reconstruction of distance distribution for noise-free model data and noisy model data (SNR ≈ 850) using the new SVD method. (A) Model dipolar signal; (B) model dipolar signal with added noise (see added noise in red plot); (C) singular value cutoff at each distance (nm) for the model dipolar signal; (D) singular value cutoff at each distance (nm) for the model dipolar signal with added noise; and (E) Distance distribution reconstructed from the model dipolar signal and model dipolar signal with noise using the singular value cut-offs shown in C and D, respectively. Note that the added noise is so small that A and B still appear identical, but convergence to the virtually identical final results requires segmentation in the latter case.

Alternatively, one can study the Piccard plot using eq 6 to identify segments and to obtain singular value cut-offs for each segment. In the Piccard plot, segments represented by the regions of r will collectively diverge at different SVCs, informing about the number of segments needed. A singular value cutoff for each of the segments can then be independently calculated by adding the SVC's for the jth segment to locate the onset of divergences occurring at $q_j + 1$, thereby giving the correct q_j for each segment. This approach is the more convenient and lends itself to automation in programming.

We tested the new SVD method on model data as well as experimental data from ref 14 and compared it with the TIKR method as well as with TIKR followed by the maximum entropy method (MEM)[8] (see Figures S9–S12). The MEM method improves the fit and removes the negative values of $P(r)$. For the model cases, we used both a unimodal and bimodal Gaussian distribution with peaks respectively at 4 nm, and 4 nm and 5 nm, each having a standard deviation of 0.3 nm (see Figures S9–S10). For the bimodal case, the height of the first peak is taken as 80% of the second peak. The evolution time for both unimodal and bimodal dipolar signal is 5 μs. The initial SNR of 30 and 10, respectively, was generated using white Gaussian noise, but we just show the denoised version.

For experimental cases, we used unimodal and bimodal distributions (Figure S11 and Figure S12, respectively) generated from a T4 lysozyme (T4L) system. The sample for the unimodal distribution was spin-labeled with T4L mutant 44C/135C at 63 μM concentration. Signal was acquired for 112 and 14 min to obtain different SNRs. The sample for the bimodal distribution was spin-labeled with T4L mutant 8C/44C and 44C/135C at 44 μM and 47 μM concentration, respectively. For different SNRs, signal averaging of 48 and 8 min was carried out. The dipolar signal was obtained from double electron–electron resonance (DEER) experiments at 17.3 GHz. For further details about the experiment, see ref 14. Figures S9 to S12 show the successful application of the SVD method.

The WavPDS method was used to first denoise the model and experimental dipolar signals to obtain high SNR (see Table S1). One sees in this table that the SNRs of all the examples we used range from 488 to 3333. In all these cases, despite the very large SNRs, the segmentation method described above was necessary.

In Figure 4 we illustrate a challenging experimental case, where before denoising the SNR = 3.8, whereas after denoising it becomes 488. We also show in this figure (as well as in Figures S9–S12) that the standard TIKR+MEM of the denoised signal yields to spurious peaks, which, however, are nonexistent with the SVD method proposed here. Spurious peaks at short distances occur because the distribution has

DOI: 10.1021/acs.jpclett.7b02379
J. Phys. Chem. Lett. 2017, 8, 5648–5655

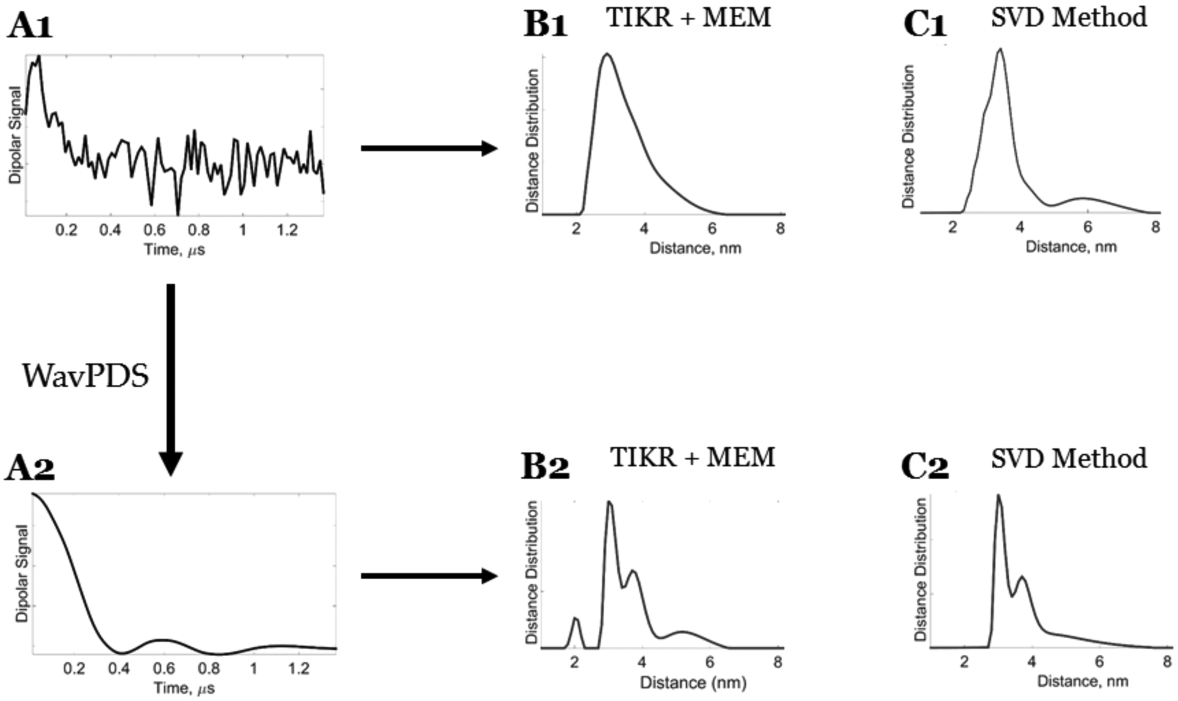

Figure 4. Reconstruction of distance distribution using Tikhonov regularization + Maximum entropy method (TIKR+MEM) and new SVD method for noisy and denoised (WavPDS) experimental dipolar signal. (A1) Noisy experimental dipolar signal from spin labeled IgE cross-linked with DNA-DNP ligand in PBS buffer solution. The dipolar signal was collected after 18 h of signal averaging and has *SNR* = 3.8; (B1) distance distribution obtained from noisy dipolar signal using TIKR+MEM; (C1) distance distribution obtained from noisy dipolar signal using new SVD method; (A2) Denoised experimental dipolar signal using WavPDS; (B2) distance distribution obtained from denoised dipolar signal using TIKR+MEM; (C2) distance distribution obtained from denoised dipolar signal using new SVD method.

diverged (become unstable) at those r values, whereas spurious peaks at long distances occur because the distribution has not converged yet at those r values. The TIKR and TIKR+MEM methods have a single singular value cutoff for all r values, which results in these spurious peaks. The new SVD method overcomes the problem by selecting different singular value cut-offs (Piccard plots: Figures S21 and S22). Also, shown in Figure 4 is the fact that before denoising, neither the TIKR+MEM, nor the new SVD method yield satisfactory results.

In summary, convergence of a SVD solution requires one to include all the "relevant" SVC's, and to exclude those that are inappropriate, and this must be performed in an r-dependent fashion to obtain optimum $P(r)$'s. We have described such a method in this Letter.

■ ASSOCIATED CONTENT

Supporting Information

The Supporting Information is available free of charge on the ACS Publications website at DOI: 10.1021/acs.jpclett.7b02379.

Details of platform and software; theorem for obtaining exact solution using SVD; Tikhonov regularization, its SVD form, and its drawback with respect to λ; orthogonality validation based on theorem for unimodal and bimodal model data; reconstructed unimodal and bimodal distance distributions of noiseless and some noise model data with different singular value cut-off; reconstructed bimodal distance distributions of noiseless and some noise model data using new SVD method; comparison of distance distributions reconstructed from TIKR, TIKR+MEM and SVD method for unimodal and bimodal dipolar signal; Piccard plots for individual r-values at each segmented region (PDF)

■ AUTHOR INFORMATION

Corresponding Author

*E-mail: jhf3@cornell.edu.

ORCID

Jack H. Freed: 0000-0003-4288-2585

Notes

The authors declare no competing financial interest.

■ ACKNOWLEDGMENTS

We would like to thank Dr. Peter Borbat and Dr. Siddarth Chandrasekaran for their valuable discussions and advice. This work was supported by the NIGMS/NIH under Grant P41GM103521.

■ REFERENCES

(1) Allen, G. I.; Peterson, C.; Vannucci, M.; Maletić-Savatić, M. Regularized Partial Least Squares with an Application to NMR Spectroscopy. *Stat. Anal. Data Min.* **2013**, *6* (4), 302−314.

(2) Borbat, P. P.; Freed, J. H. Pulse Dipolar Electron Spin Resonance: Distance Measurements. In *Structural Information from Spin-Labels and Intrinsic Paramagnetic Centres in the Biosciences*; Structure and Bonding; Springer: Berlin Heidelberg, 2013; pp 1−82.

(3) Kuramshina, G. M.; Weinhold, F.; Kochikov, I. V.; Yagola, A. G.; Pentin, Y. A. Joint Treatment of Ab Initio and Experimental Data in Molecular Force Field Calculations with Tikhonov's Method of Regularization. *J. Chem. Phys.* **1994**, *100* (2), 1414−1424.

(4) Fidêncio, P. H.; Poppi, R. J.; de Andrade, J. C. Determination of Organic Matter in Soils Using Radial Basis Function Networks and near Infrared Spectroscopy. *Anal. Chim. Acta* **2002**, *453* (1), 125−134.

(5) Tyler, B. J.; Castner, D. G.; Ratner, B. D. Regularization: A Stable and Accurate Method for Generating Depth Profiles from Angle-Dependent XPS Data. *Surf. Interface Anal.* **1989**, *14* (8), 443−450.

DOI: 10.1021/acs.jpclett.7b02379
J. Phys. Chem. Lett. 2017, 8, 5648−5655

(6) Hasekamp, O. P.; Landgraf, J. Ozone Profile Retrieval from Backscattered Ultraviolet Radiances: The Inverse Problem Solved by Regularization. *J. Geophys. Res. Atmos.* **2001**, *106* (D8), 8077−8088.
(7) Chiang, Y.-W.; Borbat, P. P.; Freed, J. H. The Determination of Pair Distance Distributions by Pulsed ESR Using Tikhonov Regularization. *J. Magn. Reson.* **2005**, *172* (2), 279−295.
(8) Chiang, Y.-W.; Borbat, P. P.; Freed, J. H. Maximum Entropy: A Complement to Tikhonov Regularization for Determination of Pair Distance Distributions by Pulsed ESR. *J. Magn. Reson.* **2005**, *177* (2), 184−196.
(9) Jeschke, G.; Chechik, V.; Ionita, P.; Godt, A.; Zimmermann, H.; Banham, J.; Timmel, C. R.; Hilger, D.; Jung, H. DeerAnalysis2006—a Comprehensive Software Package for Analyzing Pulsed ELDOR Data. *Appl. Magn. Reson.* **2006**, *30* (3−4), 473−498.
(10) Jeschke, G.; Panek, G.; Godt, A.; Bender, A.; Paulsen, H. Data Analysis Procedures for Pulse ELDOR Measurements of Broad Distance Distributions. *Appl. Magn. Reson.* **2004**, *26* (1−2), 223−244.
(11) Edwards, T. H.; Stoll, S. A Bayesian Approach to Quantifying Uncertainty from Experimental Noise in DEER Spectroscopy. *J. Magn. Reson.* **2016**, *270*, 87−97.
(12) Horn, R. A.; Johnson, C. A. *Matrix Analysis*, 1st ed.; Cambridge University Press: New York, 1985.
(13) Srivastava, M.; Anderson, C. L.; Freed, J. H. A New Wavelet Denoising Method for Selecting Decomposition Levels and Noise Thresholds. *IEEE Access* **2016**, *4*, 3862−3877.
(14) Srivastava, M.; Georgieva, E. R.; Freed, J. H. A New Wavelet Denoising Method for Experimental Time-Domain Signals: Pulsed Dipolar Electron Spin Resonance. *J. Phys. Chem. A* **2017**, *121* (12), 2452−2465.
(15) Borbat, P. P.; Freed, J. H. Measuring Distances by Pulsed Dipolar ESR Spectroscopy: Spin-Labeled Histidine Kinases. *Methods Enzymol.* **2007**, *423*, 52−116.
(16) Georgieva, E. R.; Borbat, P. P.; Ginter, C.; Freed, J. H.; Boudker, O. Conformational Ensemble of the Sodium-Coupled Aspartate Transporter. *Nat. Struct. Mol. Biol.* **2013**, *20* (2), 215−221.
(17) Jeschke, G. DEER Distance Measurements on Proteins. *Annu. Rev. Phys. Chem.* **2012**, *63* (1), 419−446.
(18) Klare, J. P.; Steinhoff, H.-J. *Structural Information from Spin-Labelled Membrane-Bound Proteins*; Springer: Berlin Heidelberg, 2013; pp 205−248.
(19) Mchaourab, H. S.; Steed, P. R.; Kazmier, K. Toward the Fourth Dimension of Membrane Protein Structure: Insight into Dynamics from Spin-Labeling EPR Spectroscopy. *Structure* **2011**, *19* (11), 1549−1561.
(20) Edwards, D. T.; Huber, T.; Hussain, S.; Stone, K. M.; Kinnebrew, M.; Kaminker, I.; Matalon, E.; Sherwin, M. S.; Goldfarb, D.; Han, S. Determining the Oligomeric Structure of Proteorhodopsin by Gd3+-Based Pulsed Dipolar Spectroscopy of Multiple Distances. *Structure* **2014**, *22* (11), 1677−1686.
(21) DeBerg, H. A.; Bankston, J. R.; Rosenbaum, J. C.; Brzovic, P. S.; Zagotta, W. N.; Stoll, S. Structural Mechanism for the Regulation of HCN Ion Channels by the Accessory Protein TRIP8b. *Structure* **2015**, *23* (4), 734−744.
(22) Schiemann, O.; Prisner, T. F. Long-Range Distance Determinations in Biomacromolecules by EPR Spectroscopy. *Q. Rev. Biophys.* **2007**, *40* (1), 1.
(23) Borbat, P. P.; Mchaourab, H. S.; Freed, J. H. Protein Structure Determination Using Long-Distance Constraints from Double-Quantum Coherence ESR: Study of T4 Lysozyme. *J. Am. Chem. Soc.* **2002**, *124* (19), 5304−5314.
(24) Hansen, P. C.; O'Leary, D. P. The Use of the L-Curve in the Regularization of Discrete Ill-Posed Problems. *SIAM J. Sci. Comput.* **1993**, *14* (6), 1487−1503.
(25) Raitsimring, A.; Salikhov, K. Electron Spin Echo Method as Used to Analyze the Spatial Distribution of Paramagnetic Centers. *Bull. Magn Reson* **1985**, *7* (4), 184−217.
(26) Milov, A. D.; Maryasov, A. G.; Tsvetkov, Y. D. Pulsed Electron Double Resonance (PELDOR) and Its Applications in Free-Radicals Research. *Appl. Magn. Reson.* **1998**, *15* (1), 107−143.
(27) Milov, A. D.; Tsvetkov, Y. D.; Formaggio, F.; Oancea, S.; Toniolo, C.; Raap, J. Aggregation of Spin Labeled Trichogin GA IV Dimers: Distance Distribution between Spin Labels in Frozen Solutions by PELDOR Data. *J. Phys. Chem. B* **2003**, *107* (49), 13719−13727.
(28) Stein, R. A.; Beth, A. H.; Hustedt, E. J. A Straightforward Approach to the Analysis of Double Electron−Electron Resonance Data. *Methods Enzymol.* **2015**, *563*, 531−567.
(29) Dalmas, O.; Hyde, H. C.; Hulse, R. E.; Perozo, E. Symmetry-Constrained Analysis of Pulsed Double Electron−Electron Resonance (DEER) Spectroscopy Reveals the Dynamic Nature of the KcsA Activation Gate. *J. Am. Chem. Soc.* **2012**, *134* (39), 16360−16369.
(30) Pannier, M.; Schädler, V.; Schöps, M.; Wiesner, U.; Jeschke, G.; Spiess, H. W. Determination of Ion Cluster Sizes and Cluster-to-Cluster Distances in Ionomers by Four-Pulse Double Electron Electron Resonance Spectroscopy. *Macromolecules* **2000**, *33* (21), 7812−7818.
(31) Sen, K. I.; Logan, T. M.; Fajer, P. G. Protein Dynamics and Monomer−Monomer Interactions in AntR Activation by Electron Paramagnetic Resonance and Double Electron−Electron Resonance †. *Biochemistry* **2007**, *46* (41), 11639−11649.
(32) Masureel, M.; Martens, C.; Stein, R. A.; Mishra, S.; Ruysschaert, J.-M.; Mchaourab, H. S.; Govaerts, C. Protonation Drives the Conformational Switch in the Multidrug Transporter LmrP. *Nat. Chem. Biol.* **2013**, *10* (2), 149−155.
(33) Fajer, P. G.; Brown, L.; Song, L. Practical Pulsed Dipolar ESR (DEER). In *ESR Spectroscopy in Membrane Biophysics*; Springer US: Boston, MA, 2007; pp 95−128.
(34) Brandon, S.; Beth, A. H.; Hustedt, E. J. The Global Analysis of DEER Data. *J. Magn. Reson.* **2012**, *218*, 93−104.
(35) Matveeva, A. G.; Yushkova, Y. V.; Morozov, S. V.; Grygor'ev, I. A.; Dzuba, S. A. Multi-Gaussian Monte Carlo Analysis of PELDOR Data in the Frequency Domain. *Z. Phys. Chem.* **2017**, DOI: 10.1515/zpch-2016-0830.
(36) Srivastava, M.; Anderson, C. L.; Freed, J. H. A New Wavelet Denoising Method for Selecting Decomposition Levels and Noise Thresholds. *IEEE Access* **2016**, *4*, 3862−3877.
(37) Golub, G. . H.; Van Loan, C. . F. *Matrix Computations*, 4th ed.; Johns Hopkins Univesity Press: Baltimore, MD, 2013.
(38) Groetsch, C. W. *The Theory of Tikhonov Regularization for Fredholm Equations of the First Kind*; Pitman Advanced Publication Program: Boston, 1984.

DOI: 10.1021/acs.jpclett.7b02379
J. Phys. Chem. Lett. 2017, 8, 5648−5655